Astrometric Calibration of Array Detectors

S. Shaklan and S. 11. Pravdo
Jet Propulsion Laboratory
California Institute of Technology
M/S 306-388
4800 Oak Grove Drive
Pasadena, CA 91109

ABSTRACT

The high level of spatial uniformity in modern CCDs and other array detectors makes them excellent devices for astrometric and navigational systems. However, at the level of accuracy envisioned by the more ambitious projects, current technology produces devices with significant pixel registration errors. This paper describes a technique for measuring relative pixel positions to an accuracy approaching 0.001 pixel. The technique has been applied to WF/PCII CCDs which are shown to have 500 nm stcl]-arid-rcl)cat errors.

1. Introduction

Array detectors, in particular CCDs, arc proving to be excellent astrometric devices. They can be found in ground based systems,[1] and have been used for high-precision astrometry in space as well.[2] A number of groups are building CCI)-based astrometric cameras,[3,4] while others have begun to measure their dimensional and photometric stability.[5,6]

The Astrometric Imaging Telescope (AIT) is a proposed CCI)-based orbiting telescope designed to achieve an accuracy of 10 micro-arcseconds.[7,8] The point design calls for two side-by-side 4096 x 4096 CCDs with 7.5 micron pixels in the focal plane of the f/15, 1.5 m diameter Ritchey-Chr étien optics, In the focal plane, 10 micro-arcseconds (μas) corresponds to 1.1 nm, or 1/6800 pixel. To achieve this accuracy, the CCD is pulled across the image plane, creating star trails that effectively average over random pixel-to-pixel differences in quantum efficiency and quantum efficiency gradients. While the averaging also reduces sensitivity to pixel position errors, the system is still vulnerable at the 0.01 pixel level. To our knowledge, no one has characterized the spatial uniformity of a CCD or other array detector with this accuracy.

The purpose of this paper is to describe a technique for measuring relat ive pixel registration at the accuracies required for AIT. The technique is simple and inexpensive and can be used on any array detector. It is also practical for on-orbit calibration. We have performed an initial experiment to validate the theory, and show that 500 nm step-and-repeat errors exist on small WF/PCII CCD chips.

In section 2, we quantify the requirem ents on CCD uniformity as they relate to AIT. These include quantum efficiency, quantum efficiency gradients, charge transfer efficiency, and pixel registration. The first three requirements are surprisingly simple to achieve and can be measured using standard techniques. In section 3, we explain how pixel positions are measured with the required accuracy, Experimental results are given in section 4.

2. CCD Requirements

2.1. Pixel and sub-pixel requirements

As noted above, the AI'I' CCD is pulled across the image plane, forming a set of parallel star trails. Star positions are measured perpendicular to the direction of the trails. Each trail is about 4096 columns long, but the image width is 3 pixels, so there is an effective reduction factor of $\sqrt{4096/3} = 37$ in any random, uncorrelated pixel-to-pixel differences.

The requirements on knowledge of quantum efficiency (QE) and QE gradients were presented in an earlier paper.[7] Given the optical system described above, high-precision simulations of tile diffraction-l imited performance allowed us to determine that the QE of any pixel had to be known to 4% to achieve 10 μas precision on any star trail. Calibration of QE at the 4% level is trivial, even in space. Further, the relative QE calibration rail.gc requirement only extends over the image scale, or about 5 pixels, since each column of the star trail is an

independent measurement.

QE gradients, when multiplied by image gradients, give an intensity term whose sign depends on the relative slopes of the two. This biases the centroid toward or away from its true position. Our simulations show that QE gradients across a single pixel must be known to 21%. Calibration of QE gradients is not likely in space, but ground-based measurements should remain valid since the gradients are mainly due to the relative transparency of frollt-surface electrodes (in a front surface device). In back-illuminated devices, pixel gradients should be well blow the 21 % requirement.

Both the QE and QE gradient requirements assume that the processes arc random and that there arc no pixel-to-pixel correlations. For correlated effects, the knowledge requirements are reduced by $\sqrt{l_c}$, where l_c is the correlation length in pixels.

Charge transfer efficiency (ChTE) was also addressed in the previous work.[7] ChTE causes a vertical trail to be left behind as the horizontal star trail is shifted out of the CCD. The tails grow in proportion to distance from the horizontal shift register (HSR). This affects star centroids by linearly shifting them away from the HSR. Astrometric models see this as a linear vertical magnification change, an effect that does not introduce any error in the determination of the position of one star with respect to a field of background stars. ChTEs of 0.99996 cause the field to appear one milli-arcsecond larger in the vertical dimension; even linear astrometric plate scale models reduce the impact on target star position to well below 10 μas.

2.2. Pixel position require.nlc}its

For a given random, uncorrelated r.m.s. pixel displacement σ_p, the r.m.s. pixel displacement of a star trail is $\sigma_p/37$. For AIT, star trail errors should be less than 10 μas. The position of every pixel should then be known to an accuracy of' 370 μas, or 0.005 pixels. Larger scale errors see less column averaging but are partially removed by the astrometric plate scale model. This is addressed in detail in the following paragraphs.

When the pixel displacements arc random, but have a characteristic correlation length, the position knowledge requirements depend on the order of the astrometric plate scale model (linear, quadratic, or higher), the size and shape of the star field, and the power spectral density of the displacements. Any linear (and possibly quadratic) terms across the star trails arc completely removed by the model. The star trails reduce sensitivity to spatial variations by averaging over several cycles in the horizontal dimension, while acting as a spatial filter in the vertical dimension. In this section, we discuss the astrometric sensitivity to pixel displacements as a function of spatial frequency for two typical star fields.

A computer model was constructed that simulated the motion of a star field as a deformed CCD was pulled across the image plane. The star fields are shown in figure 1. In field 1, the brightest stars arc about 130 arcseconds from the target star, while field 2 is more compact. Both fields have reasonable uniformity in both x and y. The model used the Controlled Optics Modelling Package (COMP)[9] to form diffraction-limited images in the focal plane. The images were integrated in one dimension to form the line spread functions.

CCD deformations were modeled as random, uncorrelated Fourier components. The amplitudes and phases were used to analytically modify the star trail by displacing the line spread function in each column by the summed amplitudes (with proper phase) of all spatial frequencies contributing to the deformation at each pixel. The amplitudes were weighted so that in a given spatial frequency band, the r.m.s. pixel displacement Was equal to the r.m.s. displacement that one would expect for a 0.1 K random temperature fluctuation having the same spatial frequency. our results arc normalized so that they all correspond to the same r.m.s. temperature gradients. Large scale amplitudes are $1/f$ times larger than small scale ones.

The average positions of the modified star trails were computed. These were then compared to the average positions of the unmodifedtrails by fitting a linear affine model (3 terms per axis, 6 terms total) to the reference stars in each field. The astrometric error is the true (unmodified) target star position compared to the target star position predicted by the affine transformation.

Spatial frequencies were analyzed one band at a time. The astrometric error causal by a given power spectrum can be determined by integrating the power spectrum multiplied by the spectral sensitivities determined from the simulations.

Result.s arc given in figure 2 and table I. There arc Several interesting features in the figure. First, the low spatial frequen cy response for the more compact field 2 shows a peak at 49 m^{-1} (20.5 mm). This is about twice the distance from the target star to the surrounding reference stars. For larger periods, the stars have more common-mode motion. For smaller periods (assuming constant temperat ure variance at any spatial frequency, as

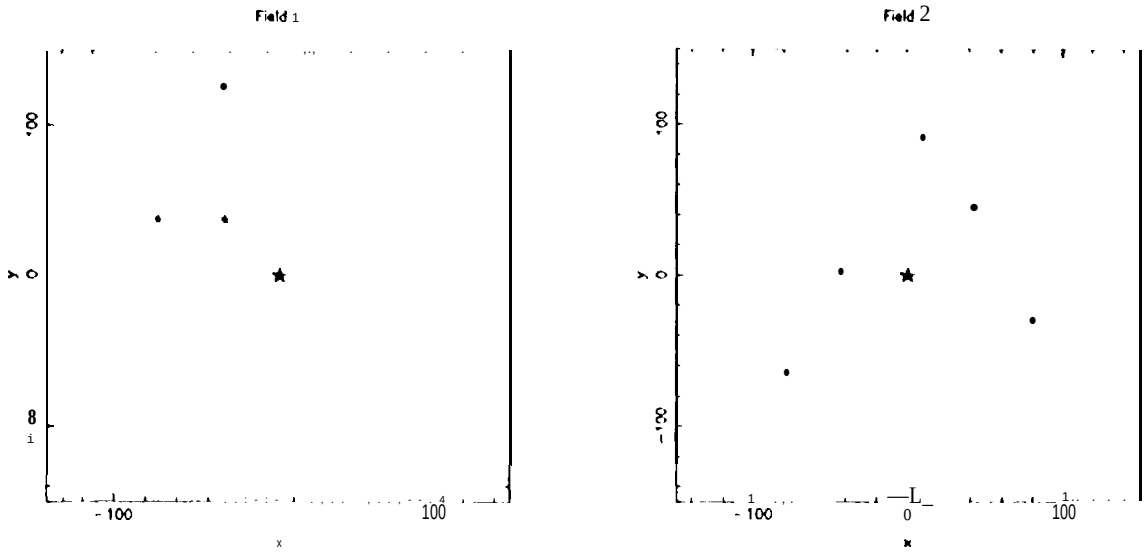

Figure 1: Star fields used for pixel displacement sensitivity study.

does the plot), the deformation amplitude decreases. One expects a minimum at about 91 m^{-1} (1 1 mm) where there is one full thermal cycle across the field. The plot shows a minimum at about 100 m^{-1}; the agreement is reasonable considering the uneven spacing of the stars. Similar arguments hold for field 1 when one accounts for the fainter stars close to the target star.

At mid-spatial frequencies, both fields show an increased sensitivity to deformations. For field '2, the peak at 140 in' ^{1}(7.1mm), is about 1.5 cycles across the 11mm wide field, indicating that this peak is similar to tile one at 49 m^{-1} (whit]) has 0.5 cycles across the field). Field 1 once again acts as if it is slightly narrower than one would expect from the distribution of brighter stars in the field.

Figure 2 shows that for low spatial frequencies, thermal fluctuations should be kept below 0.02.5 K if the target star error requirement is 10 micro-arcseconds. Larger gradients are allowed at higher spatial frequencies.

In table 1, the results of figure 2 have been reformulated to show the required accuracy on pixel position knowledge as a function of spatial frequency. The first two columns of the table are the spatial frequency and corresponding spatial period used. The third column is the r.in.s, displacement that gives 10 μas astrometric errors using the larger error of either field 1 or 2. Column 4 gives the r.in.s. calibration accuracy that must be achieved per pixel to characterize the CC]) at the required accuracy over one cycle of the spatial frequency. This implicitly assumes that the errors in each pixel are uncorrelated. (This is the case when the calibration is limited by photon statistics, for example). It was computed from the square root of the numb er of pixels/period multiplied by the accuracy per cycle.

The worst case calibration requirement in column 4 is 0.005 pixels. Thus, to adequately characterize the AIT CCD, the position of each pixel must l>e measured to 0.005 pixels. The performance at all spatial frequencies will then be better than 10 μas when the CCD is calibrated at this level.

3. Summary of Technique

3.1. Experimental Setup

The pixel-n apping technique is based on imaging of a simple sinusoidal interference pattern. Two single-mode fiber optics and a laser arc used to form the pattern. No other optics are required. The observed interference fringes are compared to a computer-generated ideal fringe pattern that accounts for the quantum-efficiency of each pixel. Photometric differences between the observed and ideal fringes are converted to shifts in the relative pixel positions.[10]

Figure 3 isa diagram of the experimental setup. Light from a He-Ne laser is injected into a single mode fiber

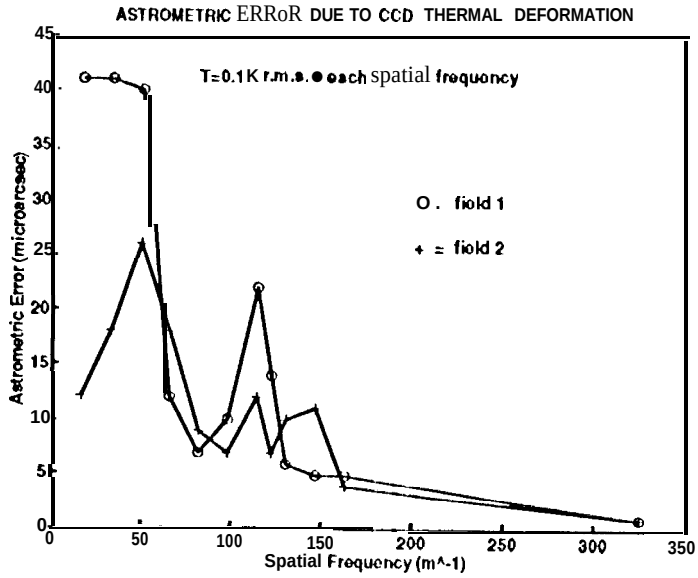

Figure 2:

'1'able 1: Astrome ic sensitivity to CCD deformations

f (m^{-1})	Period (pix)	r.m.s. for 10 μas (mm)	Single pixel knowledge reqmnt. (pix)
16.28	8192	3.8	0.049
32.55	4096	1.9	*0.016*
48.83	2730	1.3	*0.009*
65.10	2048	2.2	*0.013*
81.38	1637	3.5	0.018
97.66	1365	2.6	*0.013*
113.93	1171	1.0	*0.005*
122.00	1093	1.5	*0.007*
130.21	1024	1.9	*0.008*
146.48	911	1.5	*0.006*
162.76	819	*3.0*	*0.015*
325.52	*409*	*8.0*	*0.022*

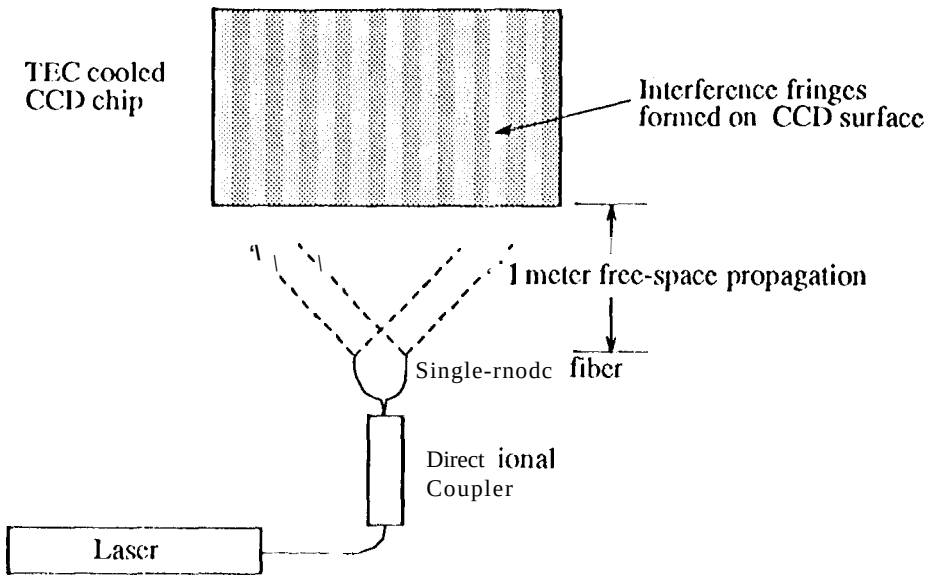

Figure 3: Experimental Setup.

and split into two fibers by a directional coupler. The two fibers are held a few mm apart in a polished block of aluminum. (The reason for polishing is explained below.) The fibers are held about 1 meter in front of the CCD so that interference fringes arc formed with a spacing of about 20 pixels on the chip. Exposures are made using both fibers simultaneously, and each fiber in turn.

A least-squares program determines the global fringe spacing, orientation, phase, amplitude, and modulation. The residuals of the optimized fit are due to either 1) poor QE calibration, 2) sub-pixel gradients, 3) CCD nonlinearities or electrical characteristics, or 4) pixel dislocations from a regular grid. Pixel dislocations are obtained as long as the QE, pixel gradient calibrations and CCD linearity have sufficient accuracy (discussed below). Figure 4 shows how pixel shifts are obtained from the least-squares residuals. A photometric difference between the optimum least-squares fit and the data is converted into a pixel shift according to the local intensity gradient. Pixel positions are measured only in the neighborhood of maximum fringe slope. (The software currently uses $\pm\pi/4$ of the midpoint). A map of the entire CCD is obtained by stitching together maps made from fringes having different phases.

Since the experiment measures the relative distances between pixels, it is not necessary to control the absolute distance between the fibers (which defines absolute pixel size), their relative optical phase (which defines the position of the CCD as a whole), or the fringe visibility (which controls sensitivity to pixel shifts). The fringes are allowed to jitter during an exposure as long as the fringe pattern in not washed out. The experimental setup is not driven by any thermal or dimensional constraints. It, is also worth emphasizing that the "flat field" calibration for this experiment is trivial. It is only necessary to measure the fibers individually (easily done by blocking one fiber at a time); it is NOT necessary to illuminate the CCD with a uniform intensity beam. Accurate flat fields arc obtained as long as the fiber beams (with FWHM ≈ 20 cm at the chip) do not wander. Shutter exposure time flue.tuatioll requirements are eased by using exposure times of a few seconds duration.

One shortcoming of using free-sl~ace propagation to form fringes between two point sources is that the interference fringes intersect the CCD along hyperbolic arcs. The hyperbola should be centered on the CCD to maintain uniform fringe spacing across the chip. Additionally, the chip should be perpendicular to the axis of the two point sources. To achieve this orientation, a laser beam is reflected between the polished block holding the fibers and the CCD. The reflected beams can easily be aligned to 0.001 radians. With this alignment precision, the fringe spacing changes by 0.0004 pixels at the edge of the CCD, while CCD tilt leads to a maximum fringe spacing difference (between the top and bottom of the chip) of 0.0003 pixel. This is well below our requirement of 0.005 pixel.

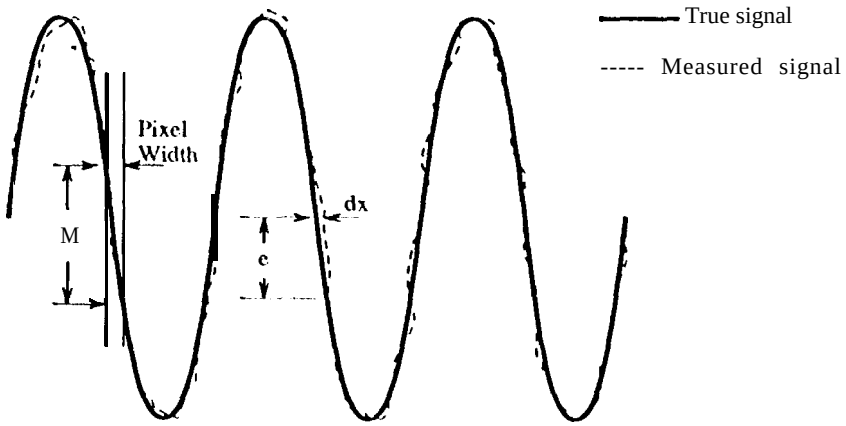

M = Signal Gradient e = Signal Error

The equivalent pixel shift is $dx = -\frac{e}{M}$ pixels

Figure 4: Converting a photometric error into a pixel registration error.

3,2. Sensitivity

The technique works by converting the photometric difference between the recorded arid ideal sine wave into a pixel registration error. As shown in figure 4, a photometric difference of e where the pixel intensity gradient is M yields a registration error of $dx = e/M$. When N photoelectrons arc recorded in a pixel, the r.in.s. noise level is $\sqrt{N}$. Thus, the noise-equivalent pixel shift is $dx = \sqrt{N}/M$.

Increasing M increases the sensitivity of the experiment. M can be increased by reducing the fringe spacing and by adding together multiple exposures. If the spacing is too small, the Iczwt-squares program (which assumes point-like pixels) introduces it's own photometric errors due to the curvature of the sine wave. A period of 10 pixels is about the minimum desired. (This can be improved by writing a least-squares program that integrates the sine wave across each pixel, but this would greatly reduce execution speed.)

For a typical fringe having .50,000 counts peak-to-peak and a period of IO pixels, the maximum gradient is $M = 15{,}700$. At mid-fringe, the amplitude is 25,000 counts and the snot noise is $\sqrt{N} = 158$ counts. In a single frame, the resulting pixel sensitivity is $dx = 0.01$ pixels. The sensitivity increases as the square-root of the number of frames averaged together. Reducing the photon-limited performance of the technique to 0.001 pixels requires on the order of 100 frames of co-added data.

3.3. Systematic errors

3.3.1. Photometric

The above disc ussion assumes that QE calibration errors do not contribute to the noise. This can be achieved by making many single-fiber exposures, so that the number of photons recorded in the "flat-field" estimation far exceeds the number of photons in the fringes.

One still poorly understood mechanism present in CCDs is diffusion of the charge among pixels. In WF/PC 11 chips, image sharpness was somewhat less than expec ted. A Kodak chip with 6.8 μm square pixels was measured and found to have a pixel response function that is significantly larger than a pixel.[11] Diffusion affects the pixel position measurements by biasing the QE calibration toward the mean QE of the chip. A relative QE error of δ leads to a pixel error of $P\delta/2\pi$, where P is the period of the fringes. With P typically set at 10 pixels, a 0.19'0 QE error manifests itself as a 0.0016 pixel position error.

Because the fringe analysis takes place in the linear portion of fringe gradients, diffusion has the same smoothing effect on the fringes that it has on the QE calibration. It reduces fringe contrast, thereby reducing sensitivity, but it dots not bias the measurements. If diffusion is not uniform or if it is intensity dependent, then biases

can exist. For non-uniformities to be significant, they must change the measured QE relative to the effective QE during exposure to the fringes, by about 0.1%.

Like diffusion, CCD nonlinearity leads to an effective QE error. Saturation should be avoided, Non-1 inearity appears as pixel errors that have the same period and orientation as the interference fringes. Thus, it is easily filtered and should not limit the sensitivity of this technique.

The sensitivity discussion also ignored A/l) resolution. An 8 bit encoder allows a sirlglc-frame resolution of 1/80 pixel, while a 1'2 bit encoder is 16 times more sensitive. Both of these figures can be improved by frame and signal averaging. Typically, the full well is small enough that the shot noise is a significant, fraction of each digitizer level. For example, when the full well is 100,000 electrons deep, the fringe midpoint is at **50,000** counts, implying an r.m. s. shot noise of **224** counts. An 8 bit encoder that spans the full well has 390 counts/level. Analysis shows that the mean value of the digitized signal will deviate by ±4 x 10^{-6} compared to the true mean as the count level moves from one digitizer level to the next. The 8 bit encoder does not limit pixel calibration at the! *0.001* level.

3.3.2. Geometric

QE gradients across individual pixels interact with the interference fringes just as they interact with images. When the gradient is in the same direction as the fringe gradient, the recorded signal is larger than one would expect based on the flat QE calibration. When the fringe gradient reverses sign, the photometric error does too. Thus, the QE gradients bias the pixel location in the same direction no matter what the fringe phase is at the pixel. The effect is indistinguishable from pixel displacements. The same is true for stellar images and star trails. In effect, the fringes are measuring the net "astrometric position" of the pixel, which is the quantity that one actually lids for astrometric calibration. To determine the true relative positions of the pixels, the QE gradients should be either 1) measured with sufficient accuracy, or **2)** the same on all pixels. Since QE gradients are mainly due to the regular pattern of electrodes across the pixels, it is likely that they are the same from pixel to pixel. At least one author has confirmed that pixel gradients repeat to 10% from pixel-to-pixel.[12]

While collecting data that are intended to be co-added, the CCD should not rotate with respect to the fibers. Rotation causes the fringes far from the center of rotation to blur. Fringe amplitude becomes a function of position, eventually causing systematic positional errors. The allowable rotation can be derived by writing the equation for fringe amplitude as a function of the relative rotation of two fringe patterns. Without going into detail here, we find that the rotational st ability requirement for 0.001 pixel calibration errors is 2 arcseconds. This is easily achieved by mounting the camera on the same optical bench as the fiber head.

4. Experimental Results

The chip being tested had the same design as standard (15 micron pixels) WF/PC 11 chips, but the pixels were 7.5 x 7.5 microns. Both small and standard WF/PC 11 chips are known to have a stc~)-ar}d-repeat error at 500 micron increments (68 rows cm the small chips). These are presumably due to either positional errors or edge effects on the 500 micron reticles used to fabricate the chips. on small WF/PC II chi ps, the 68th row appears to be approximately 6% more sensitive than the average, while on standard W F/PC 11 chips every 34th row has a sensitivity drop of about 3%.

While it has been assumed that a reticle step-and-repeat error has resulted in rows that arc either too wide or too narrow, no one has show n whether or not the effect is cumulative across the chip. The results presented here clearly show that the effect is cumulative: that is, relative to a uniform grid of pixels, the rows of small WF/PC 11 chips walk off by about -500 nm every 500 microns. The 800 x 800 small chip is about 600 nm smaller along a column than along a row.

The raw data in this experiment consisted of 8 frames each of: fringes at ≈ 45", fringes at ≈ -45°, beam 1, and beam 2. The data were recorded using an 8-bit A/D, but the gain was set so that full well occurred at 194 counts. Fringe contrast was 60%. The chip was cooled to about O °C and kept dry using a steady stream of dry N_2. The chip was not 11 used in a dewar, and there was no window. Exposure times were 2-3 seconds. Fringe spacing was about 20 pixels. Half of the chip was masked and the chip was used in a frame-transfer mode. Pixel readout, speed was 300 kpix/sec. A 300 x 300 window extending from pixel (280,80) to (579,379) was analyzed.

Measurements of the small WF/PC 11 chip snow that the st,cl)-arid-repeat error is cumulative. Figure 5 shows the average deviation of each row after subtraction of the mean pixel spacing. The pattern is explained in figure 6. The steps are about 0.07 pixels, or 525 nm large.

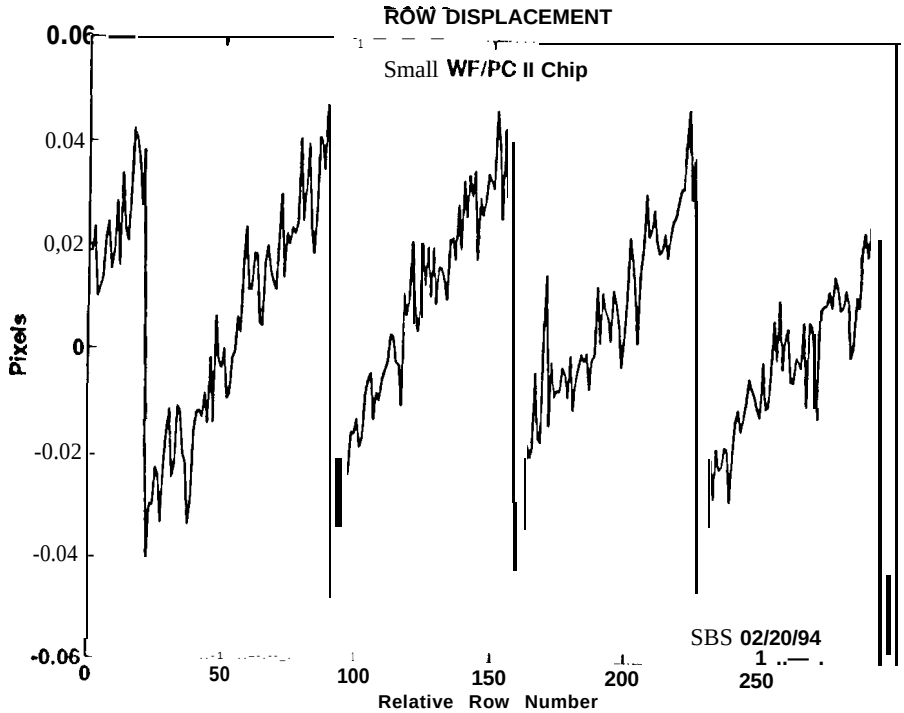

Figure 5: Step and Repeat Error of Small WF/PC II Chip

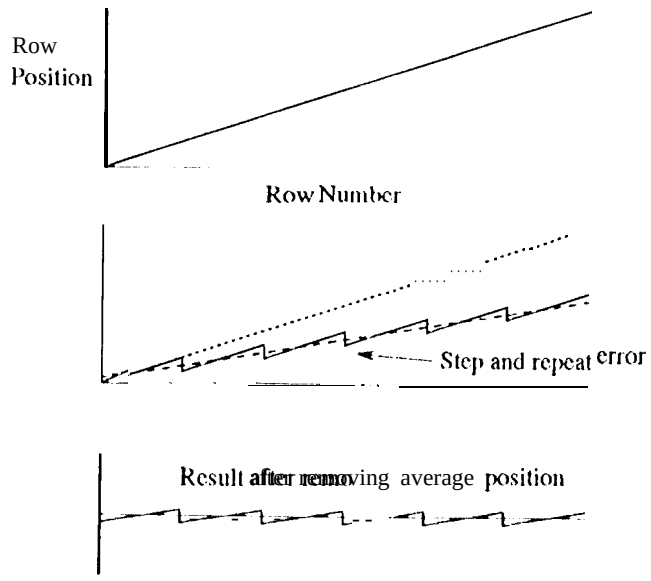

Figure 6: Explanation of figure 5.

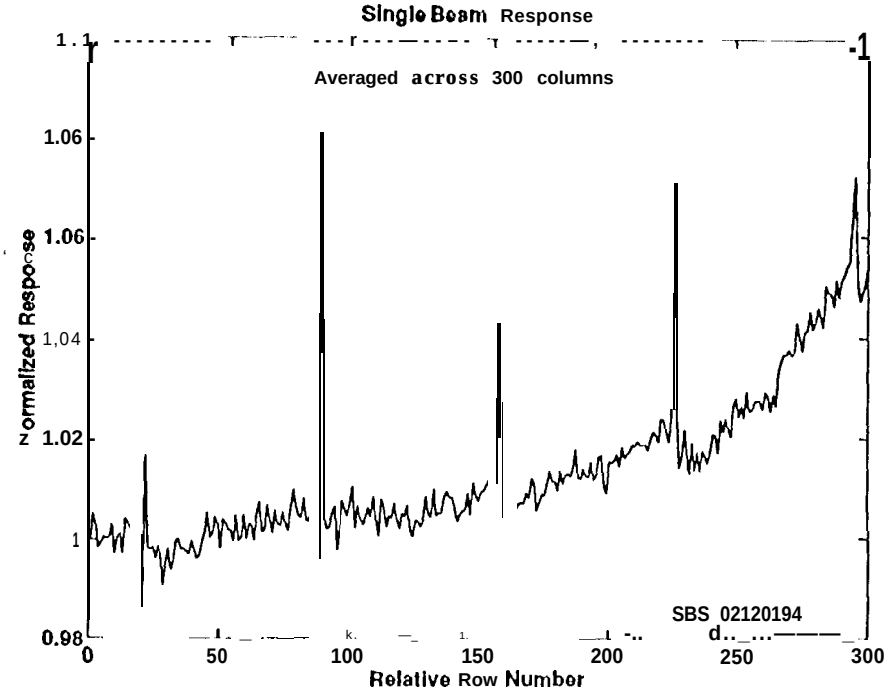

Figure 7: Response to a single fiber beam. 300 columns are averaged together. The response at the right edge may be due to non-uniformity of the beam.

The reduced data has a formal r.in.s. positional error per pixel of 0.14 pixel, When averaged across 300 columns, the error/row is 0.008 pixel. (This is the noise seen in figure 5). The high level of noise in the data set is mainly the result of 1) having only about 100 bits resolution across the fringes, 2) having a fringe amplitude of only 10,000 electrons, and 3) QE calibration errors of about 2'%. These together account for about 0.1 pixel noise. There remains a $\sqrt{2}$ difference between observed and theoretical noise that is not yet understood.

The step-and-repeat errors across the CCD occur at the locations of apparent *excess* QE (figure 7). But the signal in figure 5 indicates that the step-and-repeat error is negative in sign: groups of 68 rows are displaced by about 0.07 pixels toward the first row. One expects the pixels at step-and-repeat boundaries to have $\approx$ 7% QE drops. Note that standard WF/PC 11 chips, which were made on the same wafers as the small chips and have pixels 2 x larger, do exhibit QE drops of about 3-3.5 % every 34 pixels. This is in accord with the measurement of a negative step-and-repeat error. The QE excess of the small chips remains unexplained.

Another indicator that the step-and-repeat process is negative in sign is shown in figure 8. This is a close-up plot of the step occurring at pixel 226 in figure 5. The plot shows that the center of light of pixel 226 is shifted significantly less than those above it. This is consistent with the top edge moving by a distance dy so that its center of light moves by $dy/2$. Other boundary pixels are similar.

Yet another interesting feature of the step-and-repeat errors is that they have roughly the same magnitude across the 300 pixels that were measured. This is in contrast to the QE excesses, which varied between 2% and 8% (figure 7).

5. Conclusion

Early experimental results show that a flight-qualified CCD was manufactured with gross step-and-repeat errors. We fully expect that with further experimentation we can calibrate the entire CCD at the levels required for a high-precision astrometric mission.

We are currently buildings CCD camera that houses WF/PC II chips (large or small). The camera will be

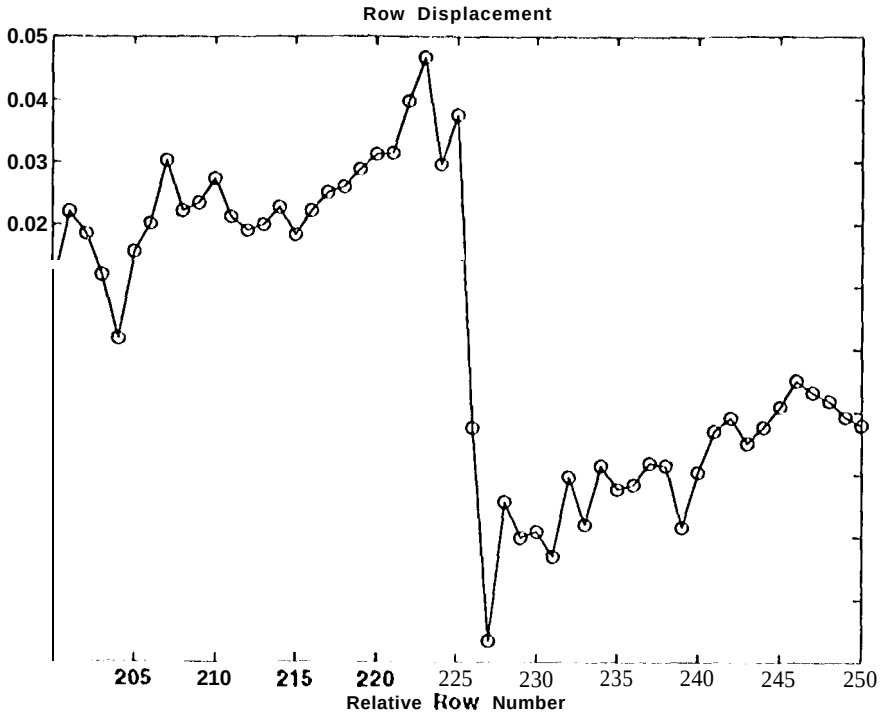

Figure 8: Close-up of the edge at pixel 226. The center of light of the boundary pixel is shifted by about 1/2 as much as the pixels above it. This shift is consistent with the pixel narrowing by 500 nm.

used for improving CCD calibration techniques, including global pixel position, sub-pixel QE gradients, and the still-mysterious WF/PC II diffusion/scattering problem. With this camera, we should achieve better than 0.005 pixel resolution per pixel. We also plan to characterize fliglit-like devices by studying large format, small-pixel chips. This chips are 4096 x 4096 and have 9 micron pixels. They have full wells of 100,000 c.- and can be used in MPP or partial-inversion mode.

We are also studying the *in situ* application of this technique for ground-based and orbiting telescopes. The two fibers would be placed in the middle of the telescope's secondary mirror (which is otherwise unused due to the central obscuration) and pointed at the CCD. A switching directional coupler would send the light of a low power laser to either fiber or split it among both. Fringes would be formed on the observing CCD just as in the laboratory experiment.

We acknowledge the assistance of S. Soll and C. Davis in collecting the raw CCD frames. The camera used is a prototype device built by S. Soll for a candidate Pluto mission instrument.

The research described in this paper was carried out at the Jet Propulsion Laboratory, California Institute of Technology. The research was partially supported by NASA through grant number AR-3574.01-91 A from the Space Telescope Science Institute, which is operated by AURA, Inc., under contract to NASA.

References

1. D. Monet, *et al*, "U.S. Naval Observatory CCD Parallaxes of Faint Stars. I - Program Description and First Results," *Astron. J.*, **103**, 638-665 (1992). There are many other examples of astrometric CCD systems described in the literature.

2. G. Null, W. Owen, and S. Synnott, "Masses and Densities of Pluto and Charon," *Astron. J.*, **105**, 2319-2335 (1993).

3. G. Gatewood, Allegheny Observatory, private communication.

4. A, Buffington, UCSD, private communication.

5. A. Buffington, 11. Hudson, and C. Booth, "A Laboratory Measurement of CCD Photometric and Dimensional Stability," *P.A.S.P*, **102, 688-697 (1990).**

6. A. Buffington, C. Booth, and H. Hudson, "Using Image Area to Control CCD Systematic Errors in Spaceborne Photometric and Astrometric '1'ilne-Series Measurements," *P.A. S. P., 103685-693* (1991),

7. S. Shaklan and S. Pravdo, "A Space-}lasd CCD Experiment for High-Precision Astrometry," *Proc. SPIE* 1945 (Orlando, 1993).

8. S. Pravdo *et* 01., "The Astrometric Imaging Telescope Optical System," *Proc. SPIE 2199* (Kona, 1994).

9. D. Redding and W. Breckinrid"Optical Modeling for Dynamics and Control Analysis,' *J.G.C.D.*, **14, 1021 (1991).**

10. This idea is based on discussions with M. Shao and an analysis by Y. Curse], who suggested that accurate measurement of the interference fringe gradients could be converted into pixel displacements. Our original idea was to illumi nate a Ronchi Ruling and spatially filter the signal. This has several disadvantages compared to the fiber scheme.

11. M. Marchywka and D. Socker, "Modulation Transfer Function Measurement Technique for Small-Pixel Detectors," *Appl. Opt.*, **31, 7198-7212 (1992).**

12. 1'. Jorden, J.M. Deltorn, and I'. Oates, "The Innermost Secrets of (X1) 5," *Newsletter R.* G. O., 41, 1-6 (1993).